

## Chapter 2

# Mechanistic Studies on Pd(OAc)<sub>2</sub>-Catalyzed *Meta*-C–H Activation Reaction

**Abstract** This chapter describes a comprehensive computational study on the template-assisted and Pd(OAc)<sub>2</sub>-catalyzed *meta*-selective C–H olefination reaction. The reaction mechanism, the active form of catalyst, the potential role of silver salt and the origin of *meta*-selectivity were investigated in this work. The computational results demonstrated that the conventionally proposed monomeric Pd(OAc)<sub>2</sub> model predicts *ortho*-selectivity, instead novel dimeric Pd<sub>2</sub>(OAc)<sub>4</sub> and Pd–Ag(OAc)<sub>3</sub> models successfully reproduce the experimentally observed *meta*-selectivity.

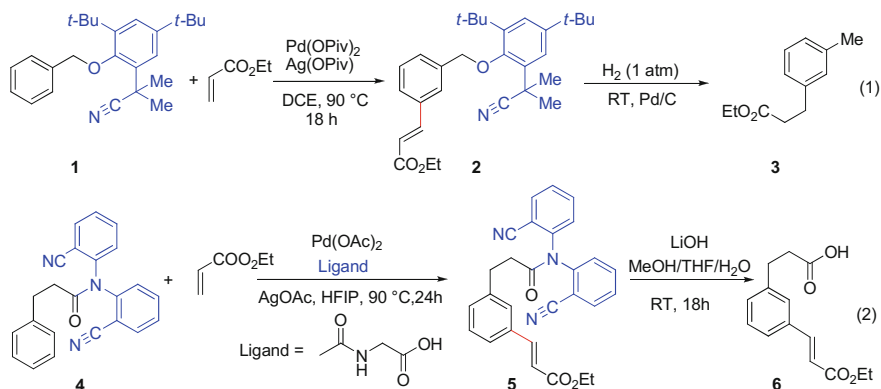
## 2.1 Introduction

Transition metal-catalyzed C–H activation reactions have received great attention in recent years [1–12]. The strategy to use directing group to increase the reactivity and control regioselectivity have been extensively applied in C–H activation reactions [13–20]. While in most of the directing group-assisted C–H activation reactions, substrate usually binds with transition metal to form a five- or six-membered cyclic transition state and active *ortho*-C–H bond selectively. A breakthrough work from the Yu group reported an ingenious template strategy for *meta*-selective C–H activation of arenes (Scheme 2.1) in 2012 [21]. In this strategy, they used end-on nitrile template to direct Pd to reach and activate *meta*-C–H bond via a macrocyclic structure. With this method, they realized *meta*-C–H activation and olefination reactions of a broad range of arene substrates including toluene derivatives and phenylpropionic acid derivatives. This new method overrides the electronic and steric bias of substrates as well as the *ortho* directing effect of chelating group to activate the remote *meta*-C–H bond which is 10 or 11

---

The results presented in this chapter have been published in the following article:

Yang, Y.-F.<sup>⊥</sup>; **Cheng, G.-J.**<sup>⊥</sup>; Liu, P.; Leow, D.; Sun, T.-Y.; Chen, P.; Zhang, X.; Yu, J.-Q.; Wu, Y.-D.; Houk, K. N. J. Am. Chem. Soc. **2014**, 136, 344. (⊥: co-first author).



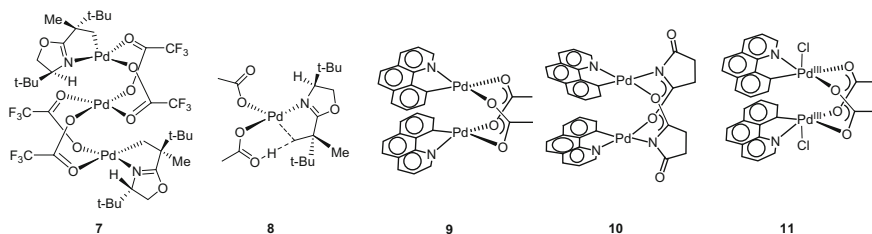
**Scheme 2.1** The first reported work about Pd(II)-catalyzed *meta*-selective C<sub>aryl</sub>–H bond activation using a removable end-on nitrile template

chemical bonds away from the directing group (nitrile group) with high selectivity. The template design concept in this work represents remarkable progress in the field of C–H activation and opens new opportunities for achieving unusual selectivities in C–H activation of arenes.

Since the Yu group's seminal work, the template strategy has rapidly been applied to a series of Pd(II)-catalyzed C<sub>aryl</sub>–H activation and functionalization to achieve *meta* and *para* selectivity [21–33]. These extensive successful examples demonstrate the enormous potential in synthetic application for this strategy. Understanding on reaction mechanism will facilitate the development of new reactions. However, its reaction mechanism and the origin of *meta*-selectivity were unclear. Therefore, we conducted mechanistic studies on reaction 1 and intended to address two critical issues: (1) what is the mechanism of reaction 1 and what is the active form of the catalyst? (2) What is the origin of *meta*-selectivity?

In regard to the active form of the catalyst, palladium catalyst can be effective in various forms [34] depending on the ligand, temperature, solvent and other reaction conditions. Despite the general mechanism of Pd-catalyzed C–H bond activation has been explored by experiments [35–40] and computations [41–47], it is still controversial about whether monomeric, dimeric or trimeric Pd is the active catalyst. In the oxazoline directed Pd-catalyzed sp<sup>3</sup> C–H activation and iodination reaction reported by the Yu group [48], they characterized the X-ray structure of the C–H activated trinuclear palladacycle complex **7**. The Houk group investigated the mechanism of this reaction [49] and found that monomeric Pd complex is the active catalyst and this trimeric intermediate is formed via a monomeric Pd transition state (**8**).

Dimeric palladium complexes are quite common in literature [50, 51]. For example, the Ritter group [52] synthesized acetate group bridged Pd<sup>II</sup>–Pd<sup>II</sup> dimeric complex [(2-phenylpyridine)Pd(μ-OAc)]<sub>2</sub> (**9**). Other dimeric palladium complexes with succinic acid (**10**) or other carboxylic acids as linker have been reported [53].



**Scheme 2.2** Trimeric and dimeric palladium complexes (**7** and **9–11**) and monomeric **TS8** reported in literature

Many of these dimeric Pd complexes are critical intermediates in  $\text{Pd}^{\text{II}}/\text{Pd}^{\text{IV}}$  catalytic cycle. High-valent binuclear  $\text{Pd}^{\text{III}}\text{--Pd}^{\text{III}}$  complexes [54] have also been developed and applied as redox catalysts for C–X reductive elimination [55]. In a recently published work by the Hartwig group [56], the C–H arylation of pyridine N-oxide is assisted by a cyclopalladated dinuclear Pd complex in which C–H bond cleavage occurs at one Pd center while the functionalization step proceeds at the second Pd center. In the study on Pd-catalyzed C–H oxidative coupling of 1,3-dimethoxybenzene with benzo[h]quinolone by Sanford and Schoenebeck and co-workers [57], both monomeric and dimeric Pd mechanisms have been investigated. Their study showed that the predicted selectivity is equivalent for carbonate and acetate, no matter whether dimeric or monomeric Pd complexes are considered and the C–H bond activation of the substrate occurs at one  $\text{Pd}^{\text{II}}$  center in their dimeric model.

Monomeric Pd complex has been extensively considered as active form for palladium catalysts. Most of mechanistic studies of palladium acetate catalyzed reactions are based on monomeric palladium complex [41–43, 58–61].

We speculated that for remote C–H activation and functionalization, the active species may be affected by the template. Thus, in the present work, we investigated several possible mechanisms involving monomeric, dimeric and trimeric palladium as active catalyst (Scheme 2.2).

## 2.2 Computational Method

All DFT calculations were carried out using Gaussian 09 program [62]. Geometry optimization was performed with B3LYP [63–66] hybrid density functional theory. LANL2DZ + f (1.472) [67, 68] basis set with effective core potential (ECP) was used for Pd, LANL2DZ + f (1.611) basis set with ECP was used for Ag, and 6-31G (d) [69, 70] basis set was used for other atoms. Frequency calculation for optimized structures was conducted at the same level of theory to verify the stationary points to be real minima (no imaginary frequency) or transition state (one imaginary frequency) and to obtain thermodynamic energy corrections. Single point energies

were calculated at M06/SDD-6-311++G(d, p) [71–74] level and the solvent effect was evaluated by using SMD solvation model [75]. The relative energies with ZPE corrections and free energies (at 363.15 K) are in kcal/mol. 3D structures are displayed with CYLView [76].

## 2.3 Results and Discussion

We first calculated the possible states of palladium acetate, i.e., trimeric, dimeric, and monomeric forms of palladium acetate. Trimeric palladium acetate is the most stable complex which is in agreement with previous experimental study [49]. Dimeric palladium complexes **B** (with four acetate bridges) and **C** (with two acetate bridges) are less stable than trimeric palladium acetate **A** by 8.1 kcal/mol and 13.8 kcal/mol, respectively. Monomeric palladium acetate **D** is also less stable than **A** by 11.8 kcal/mol. Therefore, trimeric Pd<sub>3</sub>(OAc)<sub>6</sub> was used as reference complex in the following studies (Fig. 2.1).

### 2.3.1 Monomeric Pd(OAc)<sub>2</sub> Mechanism

Monomeric Pd pathway was studied first since monomeric Pd(OAc)<sub>2</sub> was conventionally considered as active catalyst for palladium acetate catalyzed reactions in experimental and computational works. There are four commonly proposed mechanisms for transition metal-catalyzed C–H activation reactions: oxidative addition, electronic aromatic substitution (EAS), concerted metalation and deprotonation (CMD) [36, 41, 60, 77–79] and  $\sigma$ -bond metathesis. The computed activation energies of these four pathways [80] are summarized in Fig. 2.2. The oxidative addition and  $\sigma$ -bond metathesis pathways are highly unfavorable and their activation free energies are 69.5 and 54.1 kcal/mol, respectively. Trials for locating TS of EAS pathway were failed. The optimizations of TS for EAS pathway always

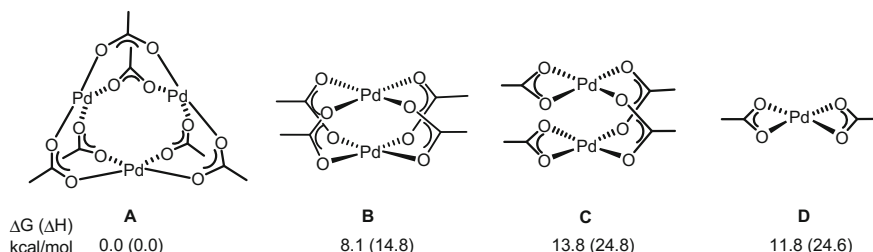


**Fig. 2.1** Trimeric, dimeric and monomeric palladium acetates and their corresponding relative free energies (electronic energies)

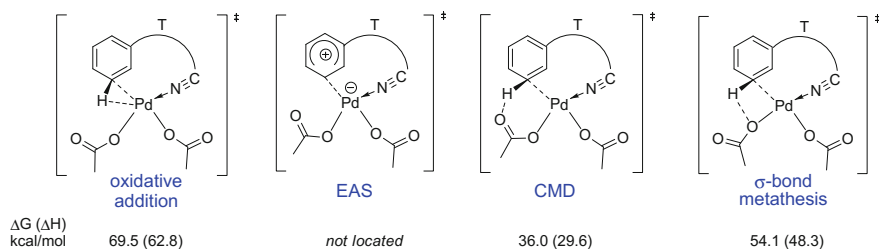
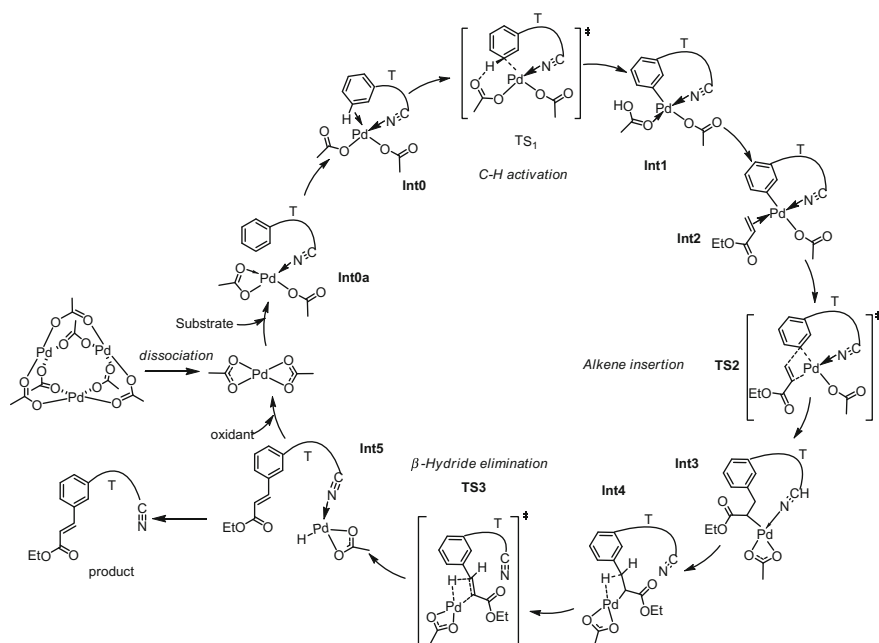


**Fig. 2.2** Four conventionally proposed reaction mechanisms for transition metal-catalyzed C–H activation and computed activation free energies (electronic energies)

converged to the intermediate with arene coordinating with Pd which indicates EAS pathway is not favorable. CMD pathway has the lowest activation energy (36.0 kcal/mol) among the four mechanisms which is in accordance with the previous study on  $\text{Pd}(\text{OAc})_2$  catalyzed C–H activation reaction [49, 81]. Thus we only considered the CMD mechanism in the following sections.

The catalytic cycle of reaction 1 is depicted in Scheme 2.3. The monomeric  $\text{Pd}(\text{OAc})_2$  is generated from the dissociation of the trimeric  $\text{Pd}_3(\text{OAc})_6$  complex. The nitrile group of substrate coordinates with Pd to form an intermediate **Int0a** and the further binding of C–H bond of the substrate with Pd leads to **Int0**. In **Int0**, the



**Scheme 2.3** Catalytic cycle of monomeric  $\text{Pd}(\text{OAc})_2$  mechanism. Reprinted with the permission from Ref. [93]. Copyright 2013 American Chemical Society

C–H bond is pre-activated via agostic interaction with Pd. After C–H bond activation step, a cyclopalladated complex **Int1** is formed. Olefin replaces acetic acetate to coordinate with Pd forming complex **Int2**. Olefination insertion followed by  $\beta$ -hydride elimination generates **Int5**. Then the product dissociates from Pd and reductive elimination releases acetic acid. Finally the Ag<sup>I</sup> oxidant oxidizes Pd<sup>0</sup> to regenerate the Pd<sup>II</sup> catalyst.

The reaction profile for monomeric Pd pathway is shown in Fig. 2.3. The formation of monomeric palladium complex **Int0a\_a** from the binding of the substrate towards trimeric Pd<sub>3</sub>(OAc)<sub>6</sub> is endothermic by 17.0 kcal/mol. The formation of **Int0\_a** requires 4.0 kcal/mol free energy from **Int0a\_a**. The C–H bond activation step needs to overcome a barrier of 36.0 kcal/mol and generates cyclopalladated complex **Int1\_a**. The replacement of acetic acid by olefin is exothermic by 5.8 kcal/mol. The olefin insertion step is a facile process with a barrier of 24.8 kcal/mol which leads to a

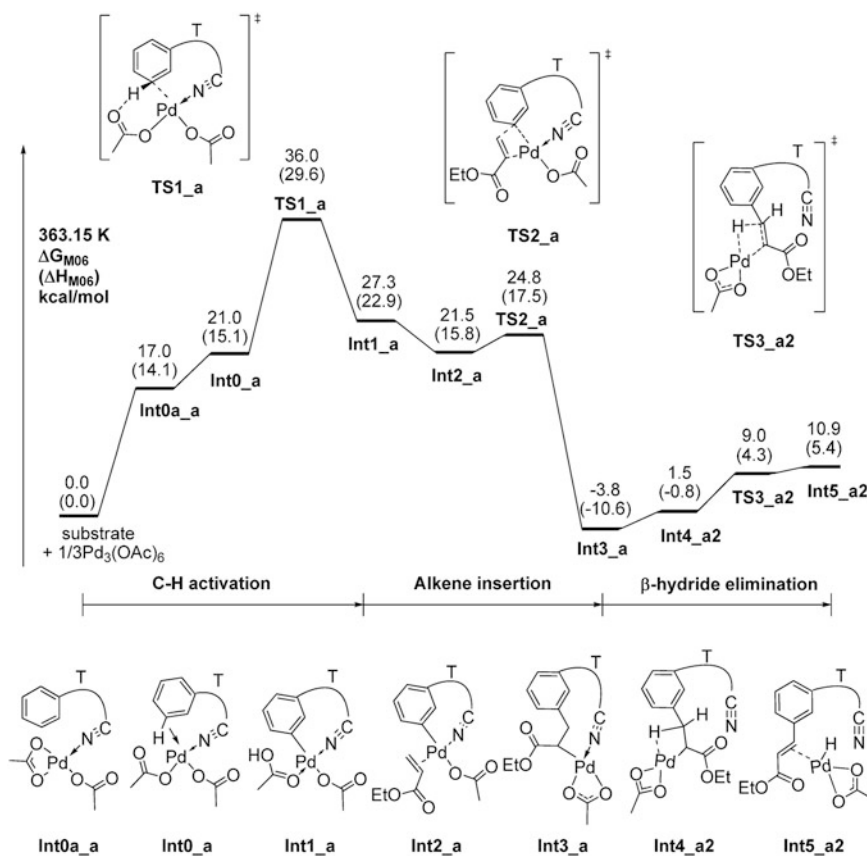


**Fig. 2.3** Energy profile for the *meta* pathway in the monomeric Pd(OAc)<sub>2</sub> mechanism. Reprinted with the permission from Ref. [93]. Copyright 2013 American Chemical Society

stable complex **Int3\_a**. The following  $\beta$ -hydride elimination step is very favorable process with a low barrier of 12.8 kcal/mol. Therefore, the C–H activation step is the rate-determining step as well as regioselectivity-determining step.

To investigate the regioselectivity, the TSs for *meta*-, *ortho*-, and *para*-C–H activation were calculated since C–H activation step is the regioselectivity-determining step. We took into account the different coordination states of the nitrile group of the substrate. As presented in Fig. 2.4(b), both TSs with nitrile coordinating with Pd (**meta\_TS1\_a**, **ortho\_TS1\_a** and **para\_TS1\_a**) and TSs without nitrile group binding with Pd (**meta\_TS1\_a2**, **ortho\_TS1\_a2** and **para\_TS1\_a2**) were calculated. It is found that in the TSs in which the nitrile group does not bind with Pd the substrate adopts a similar conformation with the ground state of the substrate (Fig. 2.4a). The dihedral angles around the C–O bond of benzyl ether in all these structures are close to 180°. Computational results demonstrate that the TS for *ortho*-C–H bond activation is more favorable than the corresponding *meta*- and *para*-TS by 1.8 and 0.8 kcal/mol, respectively, suggesting that the monomeric pathway mainly leads to *ortho*- and *para*-C–H bond functionalized products in the absence of the nitrile directing group.

In the case of the nitrile group coordinating with Pd, the activation barriers for *meta*- and *para*-TS do not change much compared to the previously discussed case without nitrile group binding to Pd. But the activation barrier of *ortho*-TS decreases significantly when the nitrile group coordinates with Pd, indicating the template promotes *ortho*-C–H bond activation for monomeric mechanism. The **ortho\_TS1\_a** is 5.9 kcal/mol lower in activation free energy than **meta\_TS1\_a**.

To understand the *ortho*-selectivity for monomeric mechanism, a further distortion-interaction analysis [82] was conducted. As shown in Scheme 2.4, the activation barrier is decomposed by an unfavorable distortion energy which is due to the conformational changes of the substrate and catalyst from reactant state to transition state and a favorable interaction between the catalyst and substrate. The system is divided into catalyst part and substrate part and their distortion energies are evaluated by the energetic differences from the reactant state to TS. Computational results (Table 2.1) demonstrate that the energetic differences of *ortho*-, *meta*-, and *para*-TS are mainly attributed to the differences in distortion energy of the substrate part. The substrate in **ortho\_TS1\_a** is less distorted (the distortion energy is 36.7 kcal/mol) while the distortion energies of substrate part for **meta\_TS1\_a** and **para\_TS1\_a** are 44.1 and 43.2 kcal/mol which are much higher than that in **ortho\_TS1\_a**. Structural analysis indicates that the greater distortion in **meta\_TS1\_a** and **para\_TS1\_a** is mainly due to the torsion about the benzyl ether C–O bond, which places two bulky groups (aryl group and benzyl group) in gauche position in the *meta*- and *para*-TS ( $\psi_3 = 78^\circ$  and  $64^\circ$ , respectively), while the two bulky groups are in anti-position in the preferred *ortho*-TS. In addition, **meta\_TS1\_a** is destabilized by the torsion about  $\psi_2$  which is enlarged from  $-101^\circ$  in reactant to  $-118^\circ$  in *meta*-TS as well as steric repulsion between the nitrogen atom of the nitrile group and the *ortho* carbon atom (N–C distance is 2.81 Å). **para\_TS1\_a** is also destabilized by steric repulsion between the ether oxygen and methyl group (O–C distance is 2.77 Å).

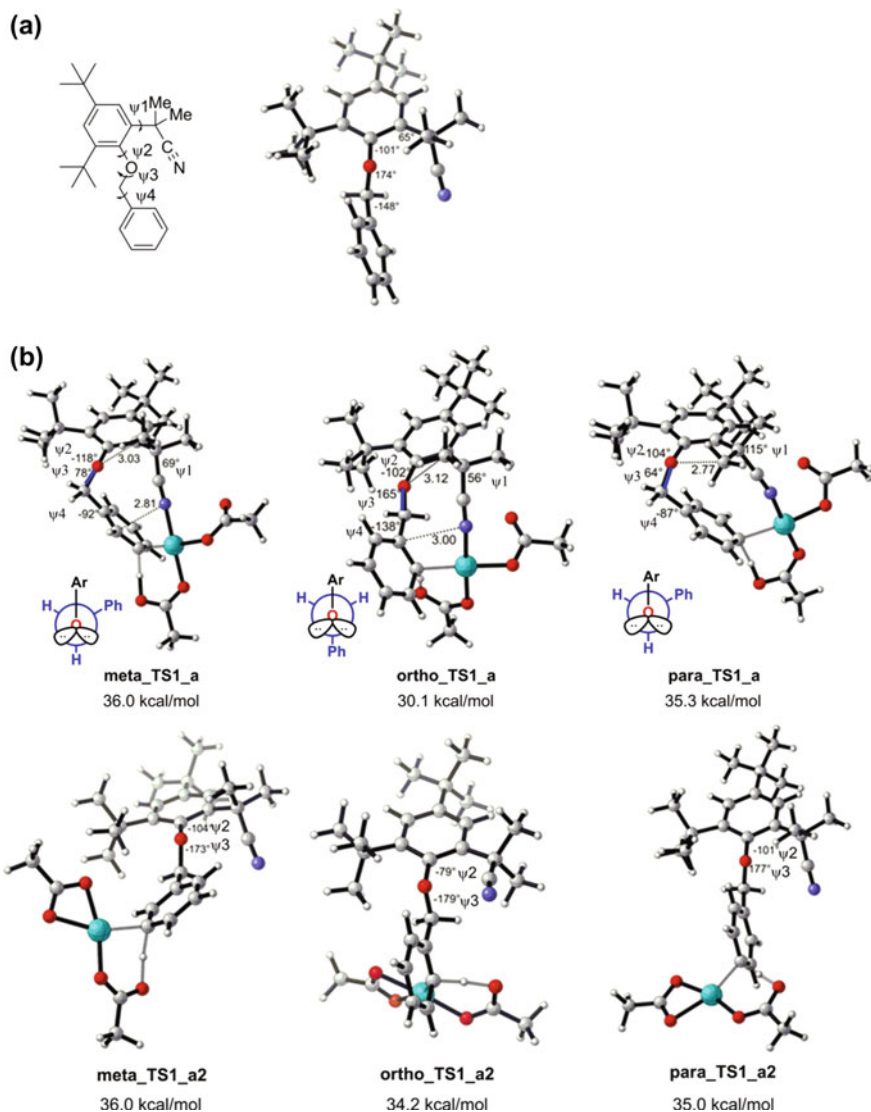
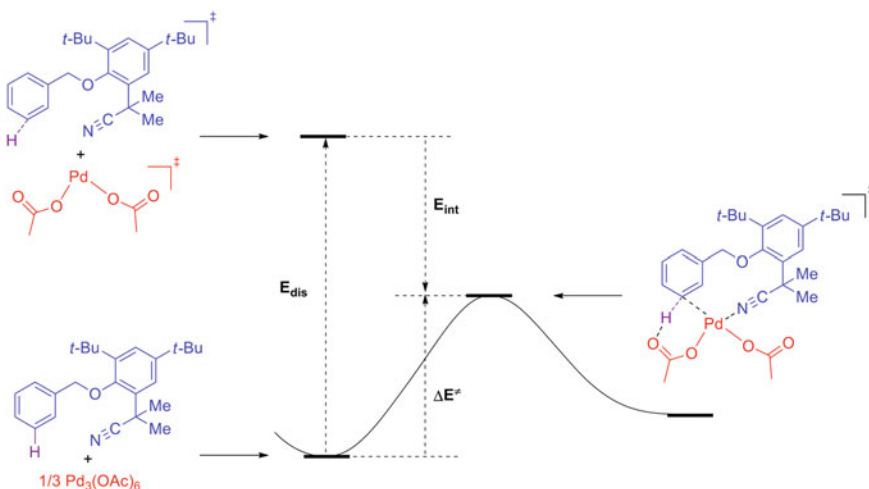


**Fig. 2.4** **a** Lowest energy conformation of toluene derivative substrate with nitrile-containing template. **b** Optimized geometries of *meta*, *ortho*, and *para* C–H activation transition states of the monomeric Pd(OAc)<sub>2</sub> mechanism. In **TS1\_a**, the nitrile group is coordinated to Pd; in **TS1\_a2**, it is not. Gibbs activation free energies with solvation correction are given in kcal/mol. Reprinted with the permission from Ref. [93]. Copyright 2013 American Chemical Society

In summary, *ortho*-selectivity is predicted by monomeric Pd(OAc)<sub>2</sub> mechanism which contradicts with the experimentally observed *meta*-selectivity (*m:p:o* = 91:7:2).



**Scheme. 2.4** Schematic diagram for distortion-interaction analysis

**Table 2.1** Distortion energy analysis of C–H activation TSs of monomeric models

Distortion energy (kcal/mol)	meta_TS1_a	ortho_TS1_a	para_TS1_a
$E_{\text{cat}}$	63.1	61.8	62.8
$E_{\text{sub}}$	44.1	36.7	43.2
$E_{\text{total}}$	107.2	98.5	106.0

### 2.3.2 Dimeric $\text{Pd}_2(\text{OAc})_4$ Mechanism

The above computational results demonstrated that the traditional monomeric Pd(OAc)<sub>2</sub> mechanism fails to explain the *meta*-selectivity of reaction 1 which impels us to investigate new mechanistic scenarios. Compared to the widely studied substrates in Pd(OAc)<sub>2</sub> catalyzed C–H bond activation reactions, substrate **1** features with a long linker which connects the remote directing group (nitrile group) and the aryl ring. The long linker enables both the directing group and the aryl group of the substrate to bind with two different Pd atoms in dimeric Pd catalyst to form a larger macrocycle. We expect that the larger macrocycle in dimeric Pd model may reduce the ring strain and distortion in *meta*-TS which destabilizes *meta*-TS in monomeric Pd model. Therefore, the present work further investigated the dimeric Pd<sub>2</sub>(OAc)<sub>4</sub> mechanism.

It is worth noting that different from the dimeric palladium acetates reported in literature which usually have two same Pd atoms (same coordination state and same functions), the two Pd atoms have different roles in the dimeric Pd model proposed

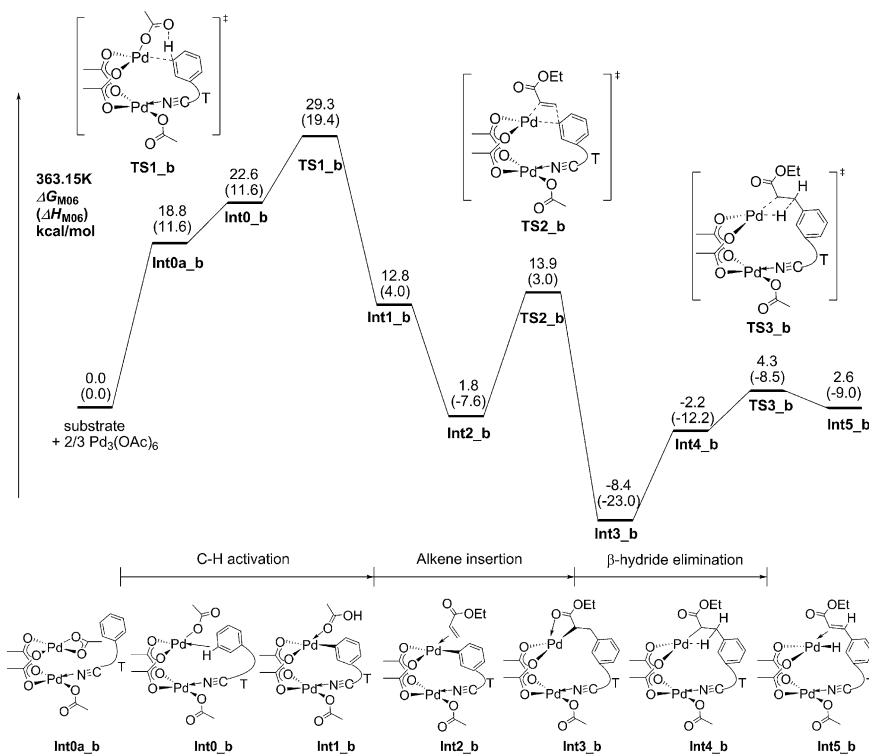


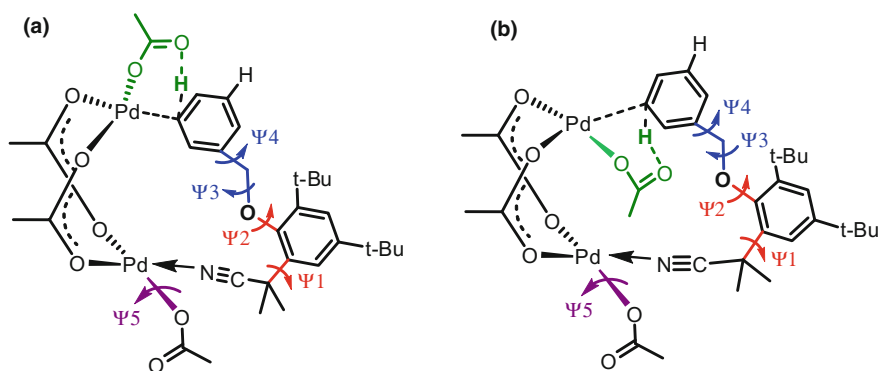
**Fig. 2.5** Energy profile for the *meta* pathway in the dimeric Pd<sub>2</sub>(OAc)<sub>6</sub> mechanism. Reprinted with the permission from Ref. [93]. Copyright 2013 American Chemical Society

in the present work. In the new dimeric Pd model one Pd coordinates with the nitrile group and another Pd coordinates with aryl group of the substrate and activates the C–H bond. Two Pd atoms are connected by two bidentate acetate groups. The computed energy profile for dimeric Pd mechanism is shown in Fig. 2.5. The C–H bond activation is also the rate-determining step and regioselectivity-determining step. The activation barrier of C–H activation for dimeric Pd model is 29.3 kcal/mol which is 6.7 kcal/mol lower than monomeric Pd model. The direct comparison of the activation energies of dimeric Pd mechanism and monomeric Pd mechanism requires a reliable computational method to precisely calculate the key interactions such as nonbonding interactions between Pd atoms, dispersion interactions in the macrocycle and the binding energy of ligand with Pd. The recently published benchmark studies have demonstrated that M06 provides reasonable accuracy to describe the ligand binding energy and dispersion energy [83–85]. We also tested the performance of M06 in calculating the dimerization energy of Pd dimer. The result with M06 method is in reasonable agreement with higher-level calculations (MP2 and CCSD(T)), suggesting it is also applicable to describe the nonbonding Pd–Pd interactions in present study [86].

We focused on the TSs of C–H bond activation since it determines the regioselectivity. For dimeric catalyst model, there are many possible conformations for intramolecular TS because it is a macrocycle (n-membered ring,  $n = 14$  (*ortho*), 15 (*meta*), 16 (*para*)). In order to search these conformations systematically, we examined the structure very carefully and identify four major factors which would lead to different conformations. As shown in Scheme 2.5, the first factor is the dihedral angles  $\Psi_1$  and  $\Psi_2$  which determines the relative position of nitrile group and the benzene ring of substrate (on the same side of the benzene ring of template or on different sides). The second factor is the dihedral angles  $\Psi_3$  and  $\Psi_4$  that determines which C–H bond of two *meta*-C–H bonds (or two *ortho*-C–H bonds) will be activated. The third factor is the rotation of the spectator acetate group (dihedral angles  $\Psi_5$ ) which brings the carbonyl above or below the Pd coordination plane. The fourth factor is the relative position of two acetate groups (green and purple in Scheme 2.5) which may locate at different sides (Scheme 2.5(a)) or the same side (Scheme 2.5(b)) of dimeric Pd catalyst.

Four variables result in 16 ( $2^4$ ) conformations for intramolecular *meta*-C–H and intramolecular *ortho*-C–H bonds activation, respectively. And eight conformations for intramolecular *para*-C–H bond activation were obtained since there is only one *para*-C–H which is not affected by the dihedral angles  $\Psi_3$  and  $\Psi_4$ . There are likewise three conformations for intermolecular C–H activation in which the nitrile group does not coordinate to the Pd center. Thus we studied 43 conformations in total. Eight favorable conformations (within a free energy window of 2.5 kcal/mol from the lowest one) are shown in Fig. 2.6.

The lowest activation barriers for *meta*-, *ortho*-, and *para*-C–H bond activation are 29.3, 29.7, and 33.4 kcal/mol, respectively, all are significantly lower than the corresponding activation barriers for counterpart TSs of monomeric Pd model. The TS for intramolecular *meta*-C–H bond activation has the lowest activation



**Scheme. 2.5** Conformations of *meta*-C–H bond activation transition state involving dimeric Pd catalyst. **a** Two acetate groups (green and purple) are on different sides. **b** Two acetate groups are positioned on the same side. Reprinted with the permission from Ref. [93]. Copyright 2013 American Chemical Society

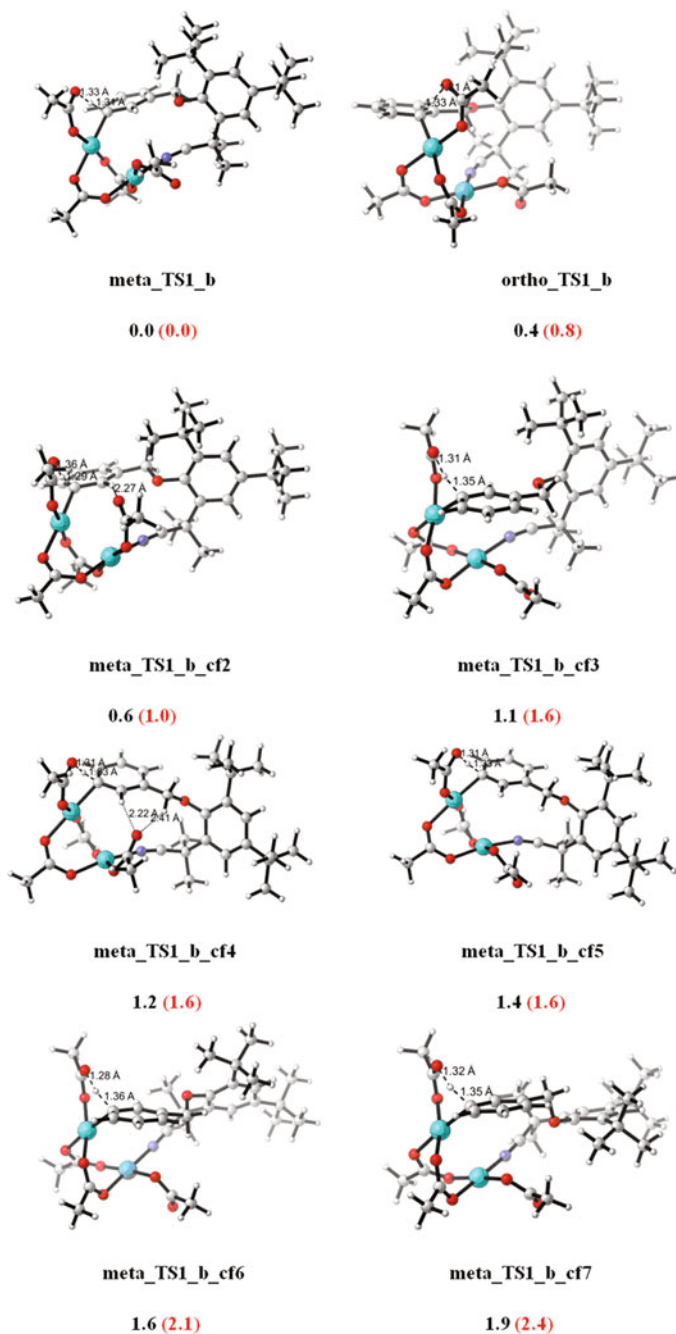


**Fig. 2.6** The favored conformations of TS (within a free energy difference of 2.0 (2.5) kcal/mol) and their relative free energies (in kcal/mol, values in black were calculated at 298.15 K and values in red parentheses were calculated at 363.15 K)

energy. It is worth noting that among these stable conformations, there are seven conformations contribute to the *meta*-C–H bond activation and only one conformation is responsible for *ortho*-C–H bond activation. According to Boltzmann distribution of these TS conformers, the ratio of *meta* and *ortho* product is estimated to be 83:17 at 363.15 K. In consideration of activation free energy and the number of stable conformations of TS, *meta*-C–H bond activation is found to be more favored than *ortho*-C–H bond activation for dimeric catalyst model. This result is in agreement with experimentally observed *meta*-selectivity.

We sought to explore the structural characters of these stable conformations and found in these stable conformations two benzene rings prefer to be mutually perpendicular and the conformations which are more close to the optimized structure of template 1 are more stable. We also found the distortion of the template 1 and the ring strain of cyclopalladated macrocycle are the key factors to influence the stability of TS.

In literature, the monomeric Pd catalyst model is frequently proposed while dimeric Pd catalyst model is less investigated. It is understandable since in most cases, the substrate is a relative small molecule and the C–H bond to be activated is always close to the directing group, thus the substrate prefers to bind with one Pd atom and the C–H bond is activated via a stable five- or six-membered cyclic TS. However, in substrate **1**, the *meta*-C–H bond is 11 chemical bonds away from the nitrile group which enables the substrate to bind with dimeric Pd to form macrocycle in which the ring strain and distortion of the substrate are released.

### 2.3.3 Dimeric Pd–Ag(OAc)<sub>3</sub> Mechanism

The oxidant screening experiment suggests that Ag(OPiv) is an optimal oxidant while other oxidants such as O<sub>2</sub> and Ag(OTf) resulted in complete loss of reactivity and selectivity. So Dr. Yang proposed the heterodimeric Pd–Ag(OAc)<sub>3</sub> catalyst model, in which the nitrile group binds to Ag and two carboxylic groups bridge Ag and Pd atoms. Pd still act as catalyst to activate the C–H bond. The crystal structure of dimeric Pd–Ag complex has been reported in literature in which Ag binds with three or four ligands. But there is no report about Pd–Ag acts as catalyst to activate C–H bond before our work published. The potential energy surface of dimeric Pd–Ag mechanism was shown in Fig. 2.7 and it indicates that the C–H bond activation step is still the rate-determining step and also the regioselectivity-determining step. The structures of the most favorable TSs are presented in Fig. 2.8. The activation barriers for dimeric Pd–Ag complex catalyzed *meta*-, *ortho*-, and *para*-C–H bond activation are 24.8, 27.8, and 28.3 kcal/mol, respectively. Therefore, dimeric Pd–Ag model also predicts *meta*-selectivity.

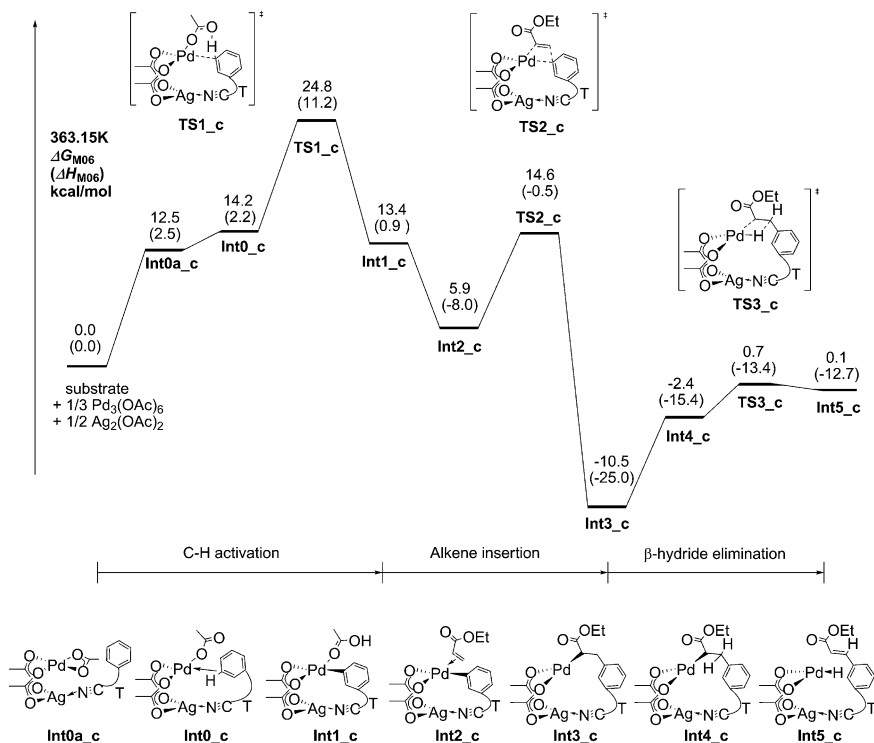


**Fig. 2.7** Energy profile for *meta* pathway in heterodimeric  $\text{Pd-Ag}(\text{OAc})_3$  mechanism. Free energies (enthalpies) are with respect to  $\text{Pd}_3(\text{OAc})_6$  and  $\text{Ag}_2(\text{OAc})_2$ . Reprinted with the permission from Ref. [93]. Copyright 2013 American Chemical Society

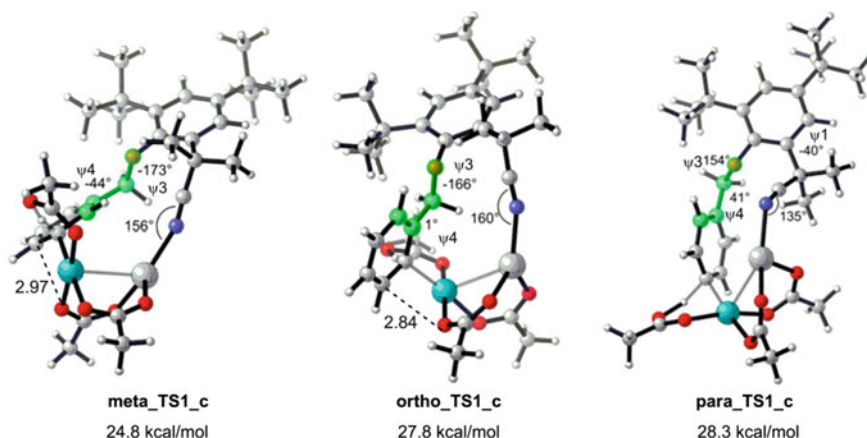


**Fig. 2.8** C–H activation transition states and activation free energies for *meta*, *ortho*, and *para* pathways of  $\text{Pd-Ag}$  (TS1\_c) dimeric mechanism. Reprinted with the permission from Ref. [93]. Copyright 2013 American Chemical Society

### 2.3.4 Trimeric $\text{Pd}_3(\text{OAc})_6$ Mechanism

Since dimeric catalyst model successfully explains the *meta*-selectivity, we further investigated trimeric catalyst model to investigate whether trimeric Pd is also reactive in C–H activation. Similar to the dimeric case, trimeric Pd catalyst model has many possible conformations resulted from the macrocyclic TS structure. We tried different TS structures including C-conformation (**TS1\_d** and **TS1\_d2**) and S-conformation (**TS1\_d3**) as well as the different coordinating status of nitrile group which are depicted in Fig. 2.9. However, they have much higher energy barriers (>37 kcal/mol) than monomeric and dimeric TSs due to greater distortions of the trimeric catalyst which indicates this trimeric catalyst model is not reasonable.

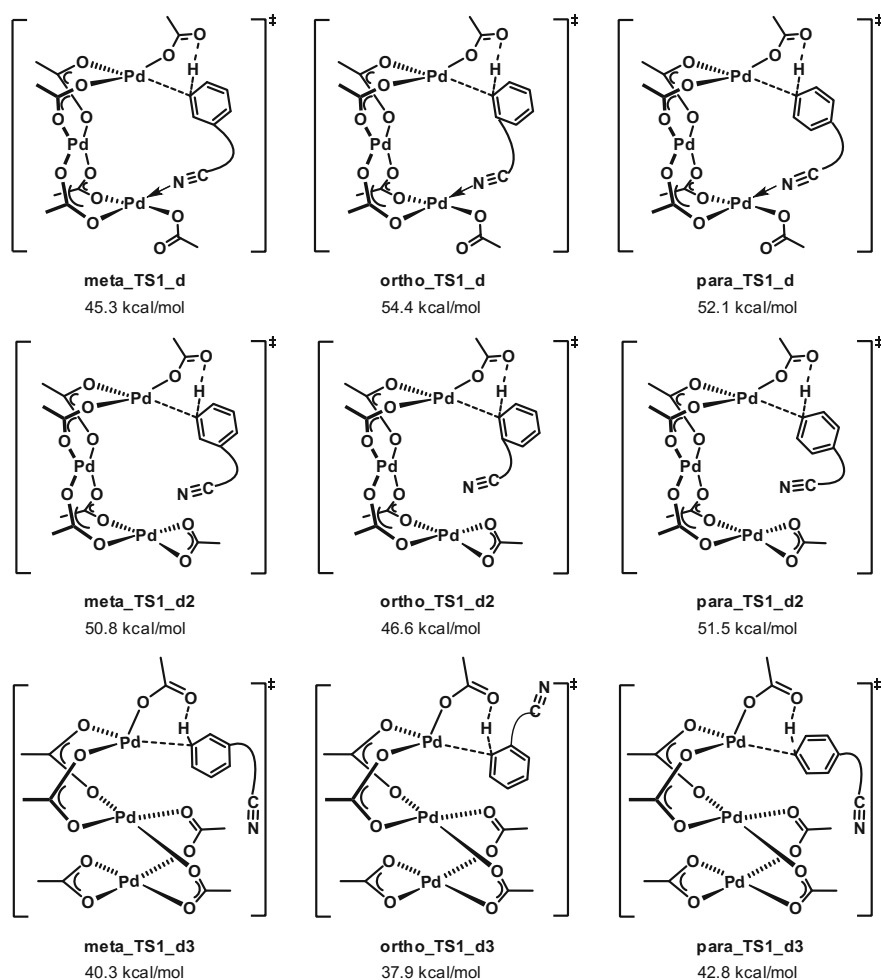
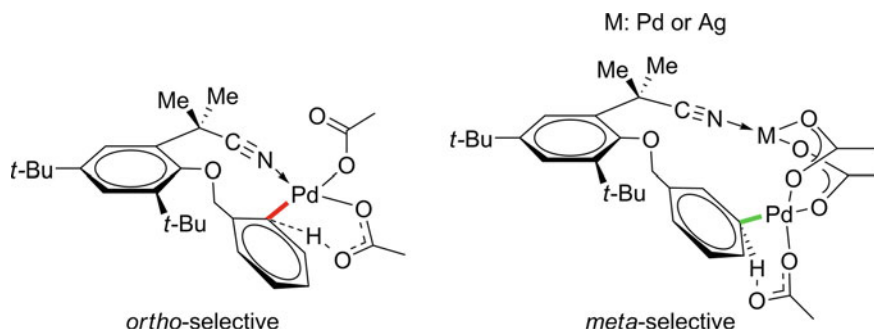


**Fig. 2.9** C–H activation transition states and activation free energies for *meta*, *ortho*, and *para* pathways of trimeric  $\text{Pd}_3(\text{OAc})_6$  mechanism



**Scheme. 2.6** Monomeric and dimeric C–H activation transition states. Reprinted with the permission from Ref. [93]. Copyright 2013 American Chemical Society

### 2.3.5 Origin of *Meta*-Selectivity in Dimeric Mechanism

One can conclude from the above computational results that both monomeric and trimeric Pd mechanisms can be ruled out since the former leads to *ortho*-selectivity and the latter has high activation barriers. The dimeric Pd–Pd and Pd–Ag models are more favorable than trimeric and monomeric Pd models in terms of activation energies and they successfully predict the experimentally observed *meta*-selectivity. Therefore, a deeper analysis on the origin of *meta*-selectivity for dimeric mechanism was performed.

As discussed in Sect. 2.3.1, in monomeric Pd model, Pd prefers to activate the *ortho*-C–H bond. Forcing the Pd to reach the remote *meta*-C–H bond will cause larger ring strain and distortion in the monomeric TS. The distortion energy of the substrate part of *meta*- and *ortho*-TS are 44.1 and 36.7 kcal/mol, respectively (Table 2.1). While in dimeric TS, the nitrile group and the activated C–H bond are bound to different Pd atoms (or Pd and Ag atoms). This special binding mode extends the size of the macrocyclic TS and directs Pd to get close to *meta*-C–H bond without introducing ring strain and torsion strain (Scheme 2.6). The distortion energy of the substrate part of *meta*- and *ortho*-TS are 33.3 and 37.7 kcal/mol, respectively (Table 2.2), demonstrating that the dimeric model significantly releases the distortion in *meta*-TS. In addition, the *meta*-TS is more flexible than *ortho*-TS in dimeric model. More low-energy *meta*-TS conformers are located in the conformational search.

**Table 2.2** Distortion energy analysis of C–H activation TSs of dimeric models

Distortion energy (kcal/mol)	meta_TS1_c	ortho_TS1_c	para_TS1_c
$E_{\text{cat}}$	35.2	36.3	36.3
$E_{\text{sub}}$	33.3	37.7	35.6
$E_{\text{total}}$	68.5	74.0	71.9

Because the TS geometries for dimeric Pd–Pd and Pd–Ag mechanism are similar, we did structural analysis for dimeric Pd–Ag model to understand the origin of *meta*-selectivity. The most stable conformations of *ortho*-, *meta*-, and *para*-TS for dimeric Pd–Ag model are shown in Fig. 2.7. **meta\_TS1\_c** has a lower activation barrier than **ortho\_TS1\_c** by 3 kcal/mol. In monomeric TS, *meta*- and *para*-TS are destabilized by the torsion strain of  $\psi_3$  (two large groups forms *gauche* conformation about the benzyl ether bond). While this unfavorable torsion strain is diminished in dimeric TSs because the larger sized macrocyclic TS allows the anti arrangement about  $\psi_3$  in all three regioisomeric transition states. On the other hand, **ortho\_TS1\_c** is destabilized by the steric repulsion between the activated benzyl ring and the ether oxygen atom ( $\psi_4 = 1^\circ$ ) as well as the repulsion between the activated benzyl group and the acetate group (C–O distance is 2.84 Å). In **meta\_TS1\_c**, these repulsions are avoided since  $\psi_4 = -44^\circ$  and the C–O distance is 2.9 Å. In addition, the C–N–Ag angle is about  $160^\circ$  in **meta\_TS1\_c** and **ortho\_TS1\_c** which is close to the value of the angle ( $180^\circ$ ) in the most favorable conformation. While this angle distorts to be  $135^\circ$  in **para\_TS1\_c**.

In order to elucidate how the substrate distortion controls the regioselectivity, a distortion-interaction analysis was performed. As shown in Table 2.2, *meta*-TS has the lowest distortion energy. It is found all the TSs have similar distortion energies in catalyst part and the major difference is from the substrate part. The substrate in **ortho\_TS1\_c** and **para\_TS1\_c** suffers greater distortion leading to higher distortion energies of 5.5 and 3.4 kcal/mol than **meta\_TS1\_c**, respectively, further supporting that the substrate distortion in the C–H activation transition states controls the regioselectivity.

## 2.4 Summary

In this chapter, we studied the reaction mechanism and regioselectivity for the palladium acetate catalyzed remote *meta*-C–H activation and olefination reaction. Possible reaction mechanisms with monomeric Pd(OAc)<sub>2</sub>, dimeric Pd<sub>2</sub>(OAc)<sub>4</sub>, dimeric Pd–Ag(OAc)<sub>3</sub>, and trimeric Pd<sub>3</sub>(OAc)<sub>6</sub> acting as active catalyst were investigated. Among these mechanisms, trimeric Pd model is ruled out due to the high activation barrier and the CMD mechanism with dimeric catalyst is found to be the most favorable mechanism. The frequently proposed monomeric Pd(OAc)<sub>2</sub> model has a higher activation barrier than dimeric models and leads to *ortho* product. Instead, the novel dimeric Pd–Pd and Pd–Ag mechanisms successfully reproduce the experimentally observed *meta*-selectivity. In the dimeric model, the nitrile group and the activated C–H are bound to two different Pd atoms of dimeric catalyst which forms a larger macrocycle. In the dimeric *meta*-TS, the large sized macrocycle direct the Pd to *meta*-C–H bond without inducing ring strain and torsion strain, thus promoting *meta*-C–H activation. This new model extends our knowledge about dimeric metal system as well as provides new ideas for the design of directing groups and new insights for the possible roles of additives used in

organic reactions. Ag(OAc)<sub>2</sub> is usually considered to act as oxidant, while our work suggests that silver salt may be involved in the active dimeric catalyst. After our work, Schaefer and co-workers [87] also proposed similar dimeric Pd–Pd and Pd–Ag models for Pd-catalyzed C–H activation reaction. Other works using dimeric catalyst or exploring the role of silver salts [88–92] have been reported recently.

## References

1. Daugulis O, Do H-Q, Shabashov D (2009) *Acc Chem Res* 42:1074
2. He J, Wasa M, Chan KSL, Shao Q, Yu J-Q (2016) *Chem Rev* DOI: [10.1021/acs.chemrev.6b00622](https://doi.org/10.1021/acs.chemrev.6b00622)
3. Chen DYK, Youn SW (2012) *Chem Eur J* 18:9452
4. Shi G, Zhang Y (2014) *Adv Synth Catal* 356:1419
5. Godula K, Sames D (2006) *Science* 312:67
6. Goldberg KI, Goldman AS (eds) (2004) *Activation and functionalization of C–H bonds*, vol 885. American Chemical Society, Washington, DC
7. Bergman RG (2007) *Nature* 446:391
8. Zheng C, You S-L (2014) *RSC advances* 4:6173
9. Chen X, Engle KM, Wang D-H, Yu J-Q (2009) *Angew Chem Int Ed* 48:5094
10. Ackermann L, Vicente R, Kapdi AR (2009) *Angew Chem Int Ed* 48:9792
11. Labinger JA, Bercaw JE (2002) *Nature* 417:507
12. Arockiam PB, Bruneau C, Dixneuf PH (2012) *Chem Rev* 112:5879
13. Rousseau G, Breit B (2011) *Angew Chem Int Ed* 50:2450
14. Horino H, Inoue N (1981) *J Org Chem* 46:4416
15. Dupont J, Consorti CS, Spencer J (2005) *Chem Rev* 105:2527
16. Yang S, Li B, Wan X, Shi Z (2007) *J Am Chem Soc* 129:6066
17. Lyons TW, Sanford MS (2010) *Chem Rev* 110:1147
18. Tremont SJ (1984) *Hayat ur. R J Am Chem Soc* 106:5759
19. Wang G-W, Yuan T-T, Wu X-L (2008) *J Org Chem* 73:4717
20. Ano Y, Tobisu M, Chatani N (2011) *Org Lett* 14:354
21. Leow D, Li G, Mei T-S, Yu J-Q (2012) *Nature* 486:518
22. Dai H-X, Li G, Zhang X-G, Stepan AF, Yu J-Q (2013) *J Am Chem Soc* 135:7567
23. Lee S, Lee H, Tan KL (2013) *J Am Chem Soc* 135:18778
24. Wan L, Dastbaravardeh N, Li G, Yu J-Q (2013) *J Am Chem Soc* 135:18056
25. Bera M, Modak A, Patra T, Maji A, Maiti D (2014) *Org Lett* 16:5760
26. Tang R-Y, Li G, Yu J-Q (2014) *Nature* 507:215
27. Yang G, Lindovska P, Zhu D, Kim J, Wang P, Tang R-Y, Movassaghi M, Yu J-Q (2014) *J Am Chem Soc* 136:10807
28. Bag S, Patra T, Modak A, Deb A, Maity S, Dutta U, Dey A, Kancherla R, Maji A, Hazra A, Bera M, Maiti D (2015) *J Am Chem Soc* 137:11888
29. Bera M, Maji A, Sahoo SK, Maiti D (2015) *Angew Chem Int Ed* 54:8515
30. Deng Y, Yu J-Q (2015) *Angew Chem Int Ed* 54:888
31. Frost CG, Paterson AJ (2015) *ACS Cent Sci* 1:418
32. Li S, Ji H, Cai L, Li G (2015) *Chem Sci* 6:5595
33. Maji A, Bhaskararao B, Singha S, Sunoj RB, Maiti D (2016) *Chem Sci* 7:3147
34. Bakhmutov VI, Berry JF, Cotton FA, Ibragimov S, Murillo CA (2005) *Dalton Trans*, 1989
35. Ryabov AD, Sakodinskaya IK, Yatsimirsky AK (1958) *J Chem Soc Dalon Trans* 2629
36. Gomez M, Granell J, Martinez MJ (1998) *Chem Soc Dalon Trans* 37
37. Dick AR, Kampf JW, Sanford MS (2005) *J Am Chem Soc* 127:12790
38. Giri R, Chen X, Yu J-Q (2005) *Angew Chem Int Ed* 44:2112

39. Powers DC, Ritter T (2009) *Nat Chem* 1:302
40. Powers DC, Geibel MAL, Klein JEMN, Ritter T (2009) *J Am Chem Soc* 131:17050
41. Davies DL, Donald SMA, Macgregor SA (2005) *J Am Chem Soc* 127:13754
42. Balcells D, Clot E, Eisenstein O (2010) *Chem Rev* 110:749
43. Garcia-Cuadrado D, Braga AAC, Maseras F, Echavarren AM (2006) *J Am Chem Soc* 128:1066
44. Rousseaux S, Gorelsky SI, Chung BKW, Fagnou K (2010) *J Am Chem Soc* 132:10692
45. Sun H-Y, Gorelsky SI, Stuart DR, Campeau L-C, Fagnou K (2010) *J Org Chem* 75:8180
46. Lafrance M, Fagnou K (2006) *J Am Chem Soc* 128:16496
47. Gorelsky SI, Lapointe D, Fagnou K (2011) *J Org Chem* 77:658
48. Chen X, Li J-J, Hao, X-S, Goodhue CE, Yu J-Q (2006) *J Am Chem Soc* 128: 78
49. Giri R, Lan Y, Liu P, Houk KN, Yu J-Q (2012) *J Am Chem Soc* 134:14118
50. Callear S, Spencer J, Patel H, Deadman J, Hursthouse M (2011) *J Chem Crystallogr* 41:523
51. Bercaw JE, Durrell AC, Gray HB, Green JC, Hazari N, Labinger JA, Winkler JR (2010) *Inorg Chem* 49:1801
52. Powers DC, Ritter T (2011) *Acc Chem Res* 45:840
53. Powers DC, Xiao DY, Geibel MAL, Ritter T (2010) *J Am Chem Soc* 132:14530
54. Cotton FA, Koshevoy IO, Lahuerta P, Murillo CA, Sanaú M, Ubeda MA, Zhao Q (2006) *J Am Chem Soc* 128:13674
55. Deprez NR, Sanford MS (2009) *J Am Chem Soc* 131:11234
56. Tan Y, Barrios-Landeros F, Hartwig JF (2012) *J Am Chem Soc* 134:3683
57. Sanhueza IA, Wagner AM, Sanford MS, Schoenebeck F (2013) *Chem Sci* 4:2767
58. Lafrance M, Gorelsky SI, Fagnou K (2007) *J Am Chem Soc* 129:14570
59. Gorelsky SI, Lapointe D, Fagnou K (2008) *J Am Chem Soc* 130:10848
60. Lapointe D, Fagnou K (2010) *Chem Lett* 39:1118
61. Gephart RT, McMullin CL, Sapiezynski NG, Jang ES, Aguila MJB, Cundari TR, Warren TH (2012) *J Am Chem Soc* 134:17350
62. Gaussian 09, Revision C.01, Frisch MJ, Trucks GW, Schlegel HB, Scuseria GE, Robb MA, Cheeseman JR Scalmani G, Barone V, Mennucci B, Petersson GA, Nakatsuji H, Caricato M, Li X, Hratchian HP, Izmaylov AF, Bloino J, Zheng G, Sonnenberg JL, Hada M, Ehara M, Toyota K, Fukuda R, Hasegawa J, Ishida M, Nakajima T, Honda Y, Kitao O, Nakai H, Vreven T, Montgomery JA Jr, Peralta JE, Ogliaro F, Bearpark M, Heyd JJ, Brothers E, Kudin KN, Staroverov VN, Kobayashi R, Normand J, Raghavachari K, Rendell A, Burant JC, Iyengar SS, Tomasi J, Cossi M, Rega N, Millam NJ, Klene M, Knox JE, Cross JB, Bakken V, Adamo C, Jaramillo J, Gomperts R, Stratmann RE, Yazyev O, Austin AJ, Cammi R, Pomelli C, Ochterski JW, Martin RL, Morokuma K, Zakrzewski VG, Voth GA, Salvador P, Dannenberg JJ, Dapprich S, Daniels AD, Farkas Ö, Foresman JB, Ortiz JV, Cioslowski J, Fox DJ (2010) Gaussian, Inc., Wallingford
63. Becke AD (1993) *J Chem Phys* 98:5648
64. Lee C, Yang W, Parr RG (1988) *Phys Rev B* 37:785
65. Becke AD (1993) *J Chem Phys* 98:1372
66. Stephens PJ, Devlin FJ, Chabalowski CF, Frisch MJ (1994) *J Phys Chem* 98:11623
67. Hay PJ, Wadt WR (1985) *J Chem Phys* 82:299
68. Roy LE, Hay PJ, Martin RL (2008) *J Chem Theory Comput* 4:1029
69. Ditchfield R, Hehre WJ, Pople JA (1971) *J Chem Phys* 54:724
70. Hariharan PC, Pople JA (1973) *Theor Chim Acta* 28:213
71. Krishnan R, Binkley JS, Seeger R, Pople JA (1980) *J Chem Phys* 72:650
72. Dolg M, Wedig U, Stoll H, Preuss H (1987) *J Chem Phys* 86:866
73. Andrae D, Häußermann U, Dolg M, Stoll H, Preuß H (1990) *Theor Chim Acta* 77:123
74. Zhao Y, Truhlar D (2008) *Theor Chem Acc* 120:215
75. Marenich AV, Cramer CJ, Truhlar DG (2009) *J Phys Chem B* 113:6378
76. Legault CY (2009) CYLView, 1.0b. Université de Sherbrooke, Canada. <http://www.cylview.org>
77. Biswas B, Sugimoto M, Sakaki S (2000) *Organometallics* 19:3895

78. Gómez M, Granell J, Martínez M (1997) *Organometallics* 16:2539
79. Tunge JA, Foresee LN (2005) *Organometallics* 24:6440
80. Ackermann L (2011) *Chem Rev* 111:1315
81. Zhang S, Shi L, Ding Y (2011) *J Am Chem Soc* 133:20218
82. Ess DH, Houk KN (2008) *J Am Chem Soc* 130:10187
83. Zhao Y, Truhlar DG (2011) *Chem Phys Lett* 502:1
84. Zhao Y, Truhlar DG (2009) *J Chem Theory Comput* 5:324
85. Zhao Y, Truhlar DG (2008) *Acc Chem Res* 41:157
86. See supporting information of ref. 93
87. Anand M, Sunoj RB, Schaefer HF (2014) *J Am Chem Soc* 136:5535
88. Hernando E, Villalva J, Martínez ÁM, Alonso I, Rodríguez N, Gómez Arrayás R, Carretero JC (2016) *ACS Catal* 6:6868
89. Senan AM, Qin S, Zhang S, Lou C, Chen Z, Liao R-Z, Yin G (2016) *ACS Catal* 6:4144
90. Whitaker D, Burés J, Larrosa I (2016) *J Am Chem Soc* 138:8384
91. Lee SY, Hartwig JF (2016) *J Am Chem Soc* 138:15278
92. Lotz MD, Camasso NM, Canty AJ, Sanford MS (2017) *Organometallics* 36:165
93. Yang Y-F, Cheng G-J, Liu P, Leow D, Sun T-Y, Chen P, Zhang X, Yu J-Q, Wu Y-D, Houk KN (2014) *J Am Chem Soc* 136:344

Mechanistic Studies on Transition Metal-Catalyzed C–H  
Activation Reactions Using Combined Mass  
Spectrometry and Theoretical Methods

Cheng, G.-J.

2017, XVII, 126 p. 95 illus., 77 illus. in color., Hardcover

ISBN: 978-981-10-4520-2